Distinct glycosylation in membrane proteins within neonatal versus adult myocardial tissue

Paolo Contessotto [a], Bradley W. Ellis [b], Chunsheng Jin [c], Niclas G. Karlsson [c], Pinar Zorlutuna [b,e], Michelle Kilcoyne [a,d] and Abhay Pandit [a]

a - CÚRAM Centre for Research in Medical Devices, *National University of Ireland Galway, Galway, Ireland*
b - Bioengineering Graduate Program, *University of Notre Dame, Notre Dame, IN, USA*
c - Department of Medical Biochemistry, *Institute of Biomedicine, Sahlgrenska Academy, University of Gothenburg, Gothenburg, Sweden*
d - Carbohydrate Signalling Group, *Microbiology, School of Natural Sciences, National University of Ireland Galway, Galway, Ireland*
e - Aerospace and Mechanical Engineering Department, *University of Notre Dame, Notre Dame, IN, USA*

Correspondence to Abhay Pandit: *abhay.pandit@nuigalway.ie*
https://doi.org/10.1016/j.matbio.2019.05.001

Abstract

Mammalian hearts have regenerative potential restricted to early neonatal stage and lost within seven days after birth. Carbohydrates exclusive to cardiac neonatal tissue may be key regulators of regenerative potential. Although cell surface and extracellular matrix glycosylation are known modulators of tissue and cellular function and development, variation in cardiac glycosylation from neonatal tissue to maturation has not been fully examined.

In this study, glycosylation of the adult rat cardiac ventricle showed no variability between the two strains analysed, nor were there any differences between the glycosylation of the right or left ventricle using lectin histochemistry and microarray profiling. However, in the Sprague-Dawley strain, neonatal cardiac glycosylation in the left ventricle differed from adult tissues using mass spectrometric analysis, showing a higher expression of high mannose structures and lower expression of complex *N*-linked glycans in the three-day-old neonatal tissue. $Man_6GlcNAc_2$ was identified as the main high mannose *N*-linked structure that was decreased in adult while higher expression of sialylated *N*-linked glycans and lower core fucosylation for complex structures were associated with ageing. The occurrence of mucin core type 2 *O*-linked glycans was reduced in adult and one sulfated core type 2 *O*-linked structure was identified in neonatal tissue. Interestingly, *O*-linked glycans from mature tissue contained both *N*-acetylneuraminic acid (Neu5Ac) and *N*-glycolylneuraminic acid (Neu5Gc), while all sialylated *N*-linked glycans detected contained only Neu5Ac.

As glycans are associated with intracellular communication, the specific neonatal structures found may indicate a role for glycosylation in the neonatal associated regenerative capacity of the mammalian heart. New strategies targeting tissue glycosylation could be a key contributor to achieve an effective regeneration of the mammalian heart in pathological scenarios such as myocardial infarction.

Introduction

Myocardial infarction (MI) consists of a massive tissue necrosis affecting cardiomyocytes located downstream in tissue no longer perfused by the recently blocked coronaries. Mammalian embryonic hearts have the capacity to regenerate [1,2] and this regenerative property is retained through the initial stages after birth but lost within the first week [3–5]. Several promising innovative therapeutic options, including gene-therapy and various biomaterial-based ones, were recently tested in clinical trials but they have not translated into an actual benefit for clinical patients yet [6,7]. Consequently, there remains an urgent clinical need for a novel effective strategy to enhance cardiomyocyte proliferation in a

post-ischemia scenario, with regeneration of tissue being the ultimate successful outcome.

All cell surfaces and extracellular matrices (ECM) are glycosylated and carbohydrates play major roles in cell-cell and cell-ECM communication and function [8]. Cell and tissue glycosylation is altered with cell differentiation and organism development [9–13] Moreover, abnormal or altered cell and tissue glycosylation is a hallmark of disease and tissue damage [14–16]. In cardiac tissue, the main cellular components of the left and right heart ventricles are comprised of the same cell types; cardiomyocytes, fibroblasts and endothelial cells, but still the precise role of each of these cellular populations is not clear during the early regenerative stage. However, the loss of the regenerative potential affects both the ventricles. Given the importance of glycosylation in biological interactions and function, specific *N*- and *O*-linked glycans could distinguish the early regenerative responses seen in the neonatal mammalian hearts and provide targets for novel tissue regeneration strategies after MI. However, a full characterisation of glycosylation differences between neonatal and mature cardiac tissue, and indeed even between left and right ventricles, is lacking at present.

In this study, the glycosylation of myocardial tissue was compared between different rat strains, left and right ventricles of mature rats and between neonatal and mature rats using lectin histochemistry and lectin microarray profiling with relative quantification. Furthermore, specific cell surface located *N*- and *O*-linked glycan structures of neonatal and adult rat were identified and quantified by mass spectrometric analysis to provide key targets for novel regenerative strategies.

Results

Glycosylation difference in sialic acid between cardiomyocytes cell surfaces and capillaries

A panel of five lectins (Table 1) was selected for their binding to general mammalian type glycosylation, i.e. sialic acid, mannose (Man) and GlcNAc (Table 1), to examine the local variation of the glycosylation within the myocardial left ventricles of both Lewis and Dark Agouti strain adult rats.

For both strains, *Maackia amurensis* agglutinin (MAA) binding was observed at the cardiomyocytes membranes which indicated the presence of terminal α-(2,3)-linked sialic acid residues on all cardiomyocyte cell surfaces (Fig. 1 F,G). *Sambucus nigra* agglutinin isolectin-I (SNA-I) binding was localised with the capillaries between the cardiomyocytes but not on cardiomyocyte cell surfaces (Fig. 1 H – I) which indicates that α-(2,6)-sialic acids are located discretely from α-(2,3)-linkages of sialic acids.

Datura stramonium agglutinin (DSA) was found to be more generic, binding both cardiomyocyte membranes and capillaries between cardiomyocytes (Fig. 1 D,E) indicating an even distribution of terminal GlcNAc in the heart tissue. Wheat germ agglutinin (WGA) bound intensely to the same cellular surfaces which were bound by DSA, (Fig. 1 A,B), consistent with its affinity for both GlcNAc but also with MAA and SNA-I binding due to WGA affinity for sialic acid regardless of linkage.

Concanavalin A lectin (ConA) is usually employed in tissue histology studies to determine the presence and localisation of *N*-linked glycosylation as it binds preferentially to α-linked mannose (Man) residues in the core structures of all *N*-linked glycans. In both left ventricles, ConA binding was localised to both the cytosolic and the membrane portion of cardiomyocytes (Fig. 1 J,K). This binding to organelles or structures is consistent with immature high mannose glycans *N*-linked glycans biosynthesised in the endoplasmic reticulum and Golgi apparatus. ConA binding to the cellular surface of cardiomyocytes was also evident but this was not extended to capillary structures, which may indicate that complex *N*-linked glycans are in higher proportion in the capillaries, as indicated by the positive staining of the other lectins. The presence of *O*-linked glycans and/or glycolipids, which do not have Man residues, is also likely to contribute to the SNA-I MAA, DSA ad WGA binding. No significant differences were seen in the binding intensity of any lectin between the two strains (Fig. 1 C), indicating a consistent glycosylation in the left ventricle between different strains.

Tissue glycosylation of adult left and right cardiac ventricles is similar across rat strains

Given the importance of glycans in the interaction with the ECM, any potential differences in the glycan composition of cardiomyocytes, which are present in the two cardiac ventricles of the heart, could be indicators of a different physiological function. Left and right ventricular tissue samples were harvested from three individuals from two different strains of healthy adult rats (Lewis and Fischer) and their membrane proteins extracted and processed specifically for the lectin microarray analysis. A heat map showing all the relative binding intensities to the lectins tested is shown in Fig. 2 A. The lectin binding profiles of both the left and right membrane proteins showed consistent high binding to WGA, SNA-I, both the isolectin I and II of *Trichosanthes japonica* (TJA), and *Ricinus communis* agglutinin (RCA-I/120). These data were consistent with the previous lectin histochemistry data that indicated the presence of complex-type glycans. High mannose-type glycan structures were detected by binding to *Lens culinaris* (Lch-B), *Calystegia sepium* (Calsepa),

Table 1. Lectins used for tissue histochemistry, their binding specificity, used concentration and inhibitory carbohydrate (150 mM).

Lectin	Abbreviation	Binding specificity	Concentration (µg/ml)	Inhibitory carbohydrate
Sambucus nigra agglutinin isolectin-I	SNA-I	Neu5Ac/Gc-α(2,6)-Gal-β(1,4)-GlcNAc-R	20	Lactose
Maackia amurensis agglutinin	MAA	Neu5Ac/Gc-α(2,3)-Gal-β(1,4)-GlcNAc-R	15	Lactose
Concanavalin A lectin	Con A	α-linked Man, Glc, or GlcNAc	20	Man
Wheat germ agglutinin	WGA	GlcNAc, Neu5Ac/Gc	10	GlcNAc
Datura stramonium agglutinin	DSA	GlcNAc	15	GlcNAc

Narcissus pseudonarcissus (NPA) and *Galanthus nivalis* (GNA) lectins. Moreover, *Phaseolus vulgaris* isolectin E (PHA-E) indicated the presence of bi- and tri-antennary complex type glycans with terminal β-linked Gal residues. Finally, terminal α-linked galactose (Gal) was present across the cardiac ventricles in both the strains, as evidenced by the binding to *Maclura pomifera* (MPA), *Vigna radiata* (VRA) and *Marasmius oreades* (MOA) lectins. Binding to *Griffonia simplicifolia* (GS) isolectin B4 indicated that at least a proportion of the terminal α-linked Gal present was a component of the terminal Gal-α-(1,3)-Gal disaccharide.

Hierarchical clustering analysis of the lectin binding intensity data highlighted an 80% similarity across all the samples tested with the exception of one left ventricle from the Fischer strain, which had a similarity of 70% with the rest of the samples, and may have represented an outlier (Fig. 2 A). None of the groups showed a clustering of all its individuals and so the individual variability did not allow the distinction of major differences due either to the ventricular or to the strain origin. Specifically, samples from both the left and right ventricles were clustered together with a total similarity percentage ranging from 80% (including all the samples apart from the outlier) to 92% related to two different samples harvested from different ventricles and strains (Fig. 2 A). Furthermore, one-way ANOVA statistical analysis confirmed the outcome of the clustering, since no significant difference was detected across the lectins that bound to high mannose- and complex-type glycans (Fig. 2 B). Therefore, glycosylation of cardiac tissues was found to be consistent between left and right ventricles also between different rat strains.

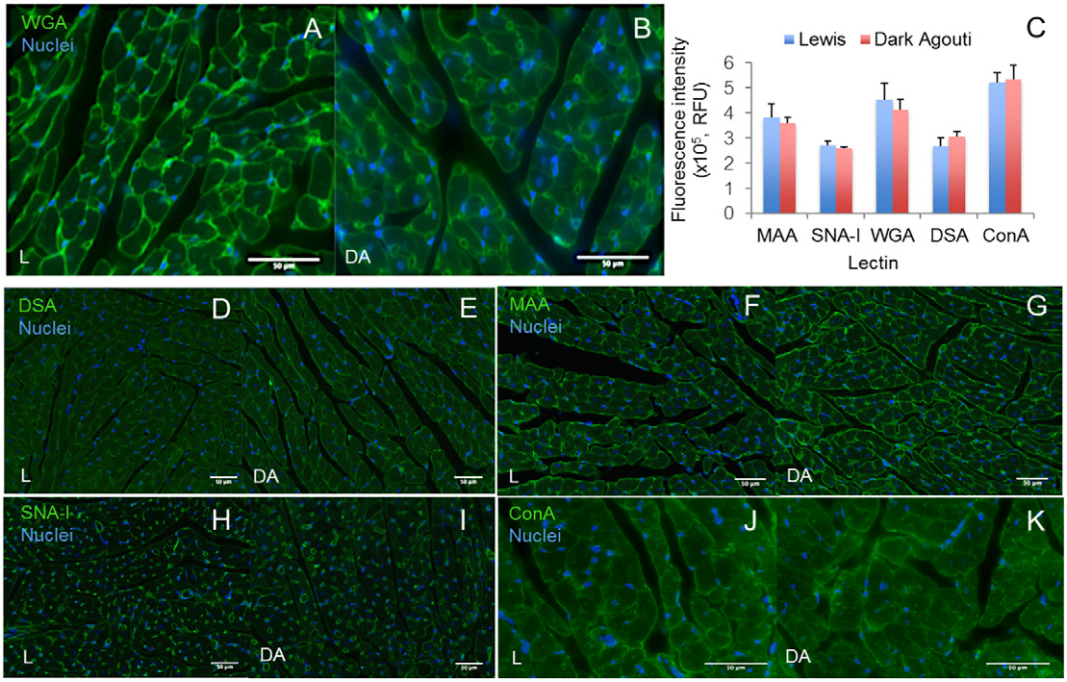

Fig. 1. Lectin binding in left ventricle and relative quantification. The same patterns were detected in both Lewis (L) and Dark Agouti (DA) rats. WGA lectin binds to sialic acid and GlcNAc residues (A,B), DSA binds to GlcNAc residues (D,E), MAA recognizes α-(2,3)-linked sialic acid (F,G), SNA-I binds to α-(2,6)-linked sialic acid (H,I) and ConA recognizes Man and Glc residues (J,K). All lectin binding intensities were background-subtracted and quantified by Image J (C). Data are shown as mean with standard deviation (n = 4–6 animals per group). Scale bar = 50 µm.

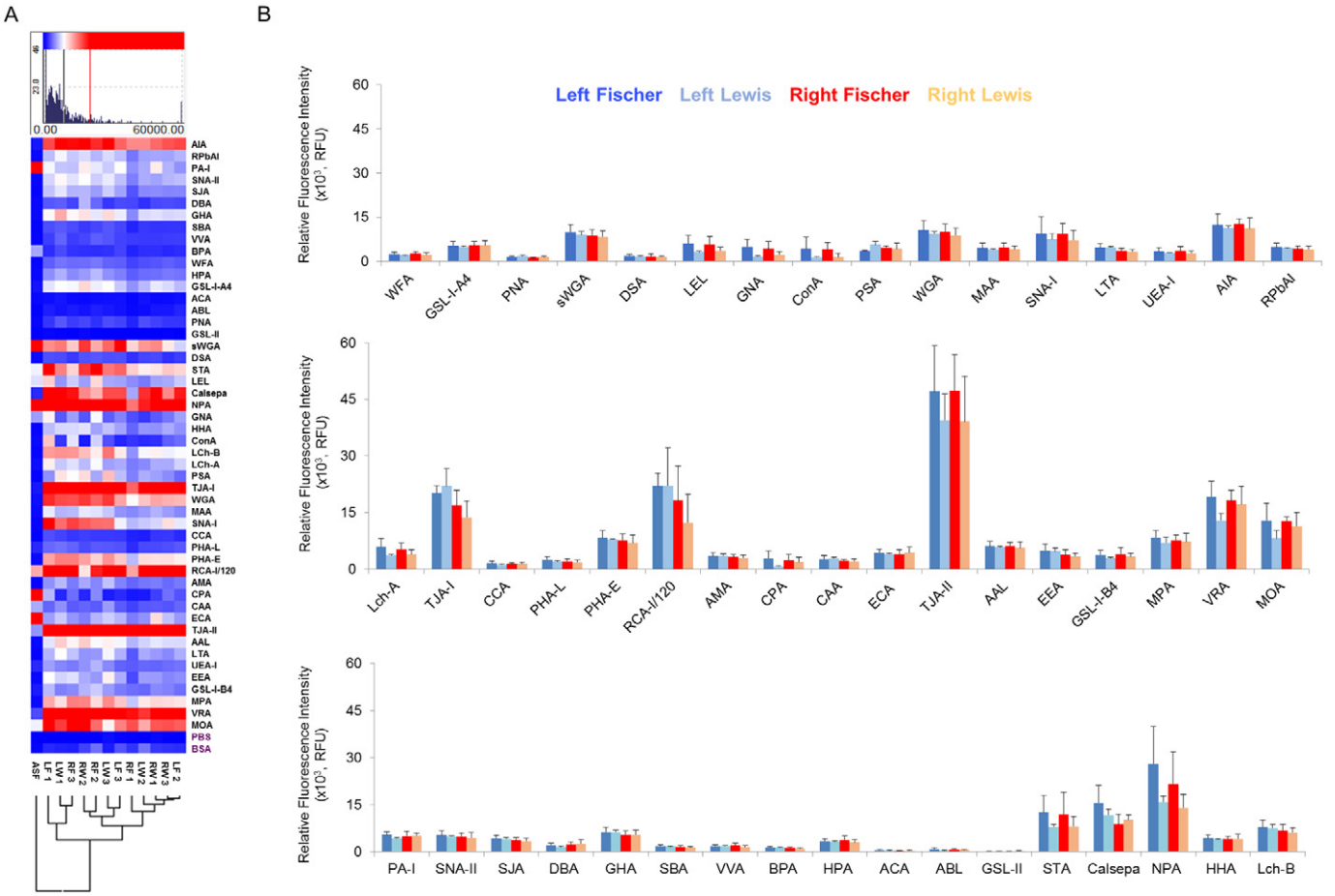

Fig. 2. Hierarchical clustering of glycan moieties detected across the left and right ventricle in two different strains of healthy rat. (A) Lectin microarrays showed the binding intensity to the glycans present in the membrane proteins extracted from the left (L) and right (R) ventricle from Fischer (F) and Lewis (W) strains of healthy rats. Hierarchical clustering showed an 80% similarity across all the samples tested with the exception of LF 1, which had a 70% similarity with the rest of the samples. Samples LF 2 and RW 3 showed a 92% similarity. Asialofetuin (ASF) was used as control glycoprotein and all lectin binding intensities were normalized. 90% laser scans were combined with 10% laser scans when intensity binding was saturated (above 60,000 RFU). (B) One-way ANOVA analysis with Tukey's post hoc correction did not identify any significant difference (n = 3 animals per group). The experiment was carried out in technical triplicate.

Complex *N*-linked and sialylated glycan structures are more abundant in adult and specific structures were detected in neonatal myocardium

In order to assess any variation between neonatal and adult heart tissue glycosylation, structural characterisation of oligosaccharides from the tissue was performed. The *N*- and *O*-linked glycan structures of Sprague Dawley healthy three-day-old and adult myocardial left ventricles were analysed by liquid chromatography-mass spectrometry (LC-MS/MS) to identify any structural variations in detail

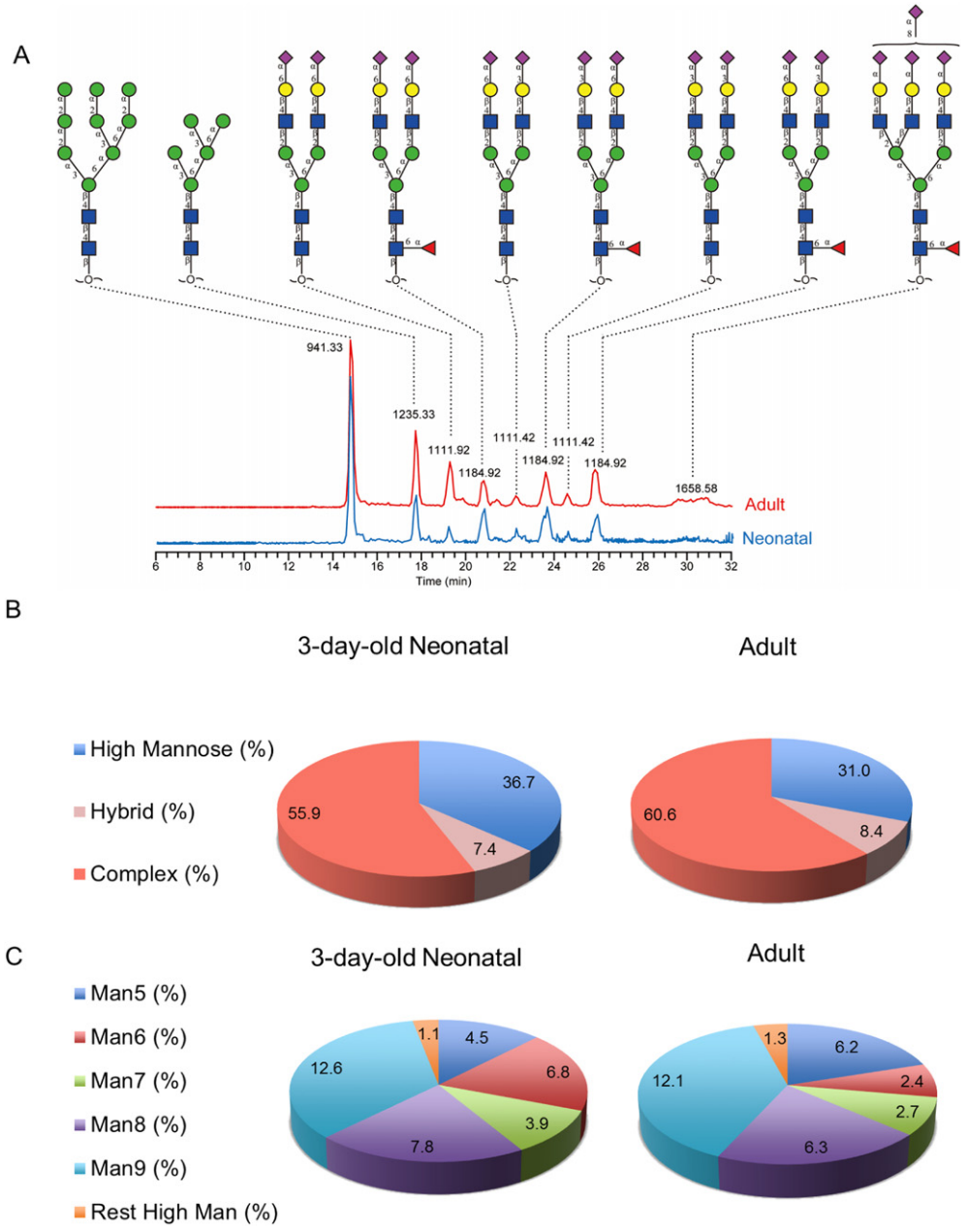

Fig. 3. Extracted ion chromatography (EIC) of the most abundant *N*-linked glycans present in the membrane protein in three-day-old neonatal and adult healthy myocardial tissue. (A) The most abundant *N*-glycans structures at *m/z* 941 ($Man_9GlcNAc_2$), 1235 ($Man_5GlcNAc_2$), 1111 ($Neu5Ac_2Hex_5GlcNAc_4$), 1184 ($Neu5Ac_2Hex_5GlcNAc_4Fuc_1$) and 1658 ($Neu5Ac_4Hex_5GlcNAc_4Fuc_1$) were chosen to show the different relative percentage of Neu5Ac-α(2,3)-Gal-, Neu5Ac-α(2,6)-Gal- and Neu5Ac-α(2,8)-Neu5Ac- in neonatal and adult left ventricular myocardial samples. (B) Adult-stage group showed a 5% increase in complex-type structures and a 6% decrease in the subgroup of high mannose structures compared to three-day-old neonatal. (C) Among total high mannose structures, $Man_6GlcNAc_2$ showed a 4% increase in relative percentage. The experiment was done using samples pooled from three different animals (n = 3 animals per group).

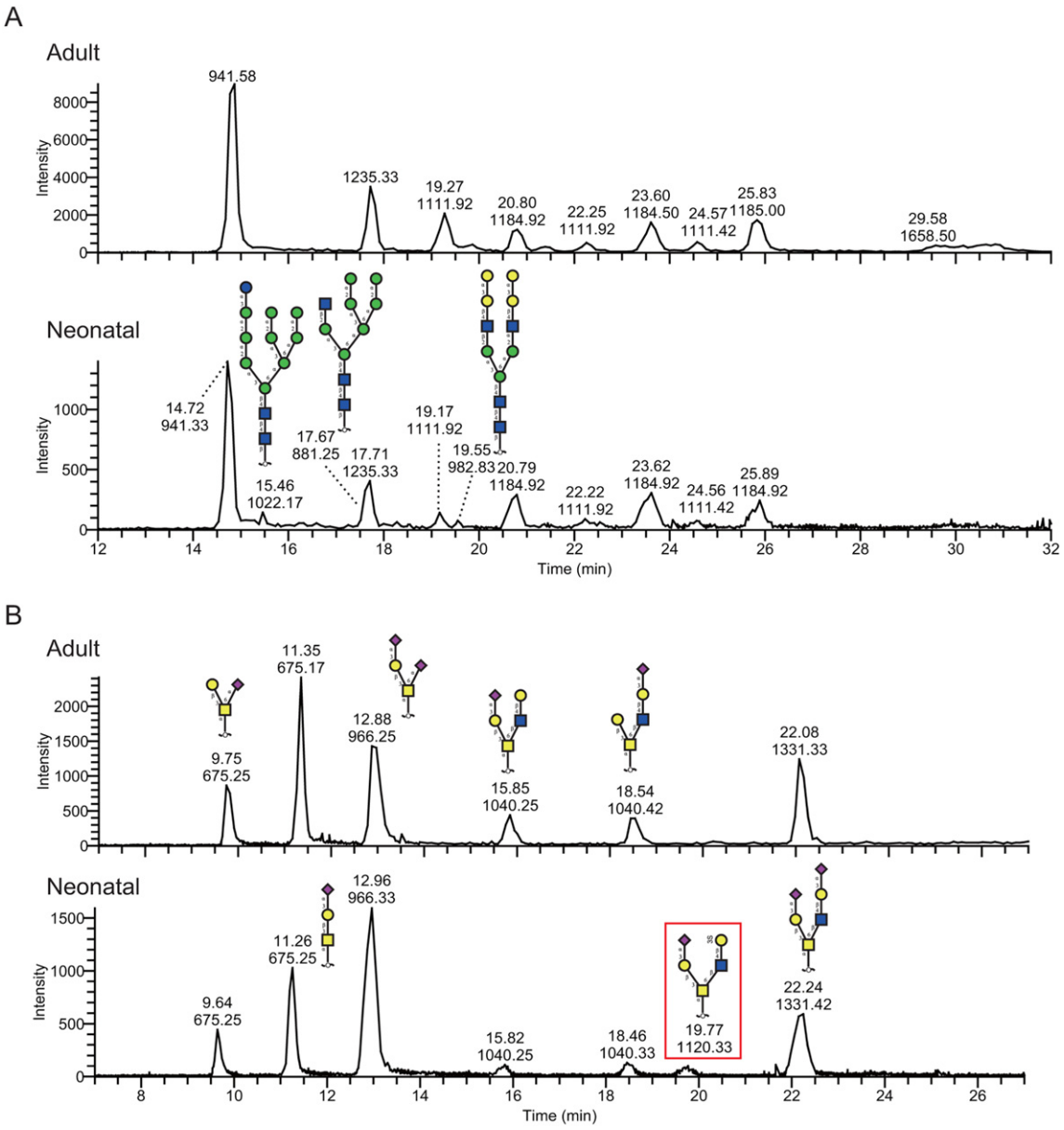

Fig. 4. Extracted ion chromatography (EIC) of *N*- and *O*-linked glycans present in the membrane protein in neonatal and adult healthy myocardial tissue. (A) Three specific *N*-glycan structures were detected in left ventricular myocardial neonatal sample at m/z 1022 ($[M\text{-}2H]^{2-}$ ions, high-mannose precursor), 881 ($[M\text{-}2H]^{2-}$ ions, hybrid-type), and 982 ($[M\text{-}2H]^{2-}$ ions, complex-type). (B) EIC of dominant core 1 and 2 *O*-glycans, one sulfated core 2 *O*-glycan ($[M\text{-}H]^{-}$ ions at m/z 1120) was detected in neonatal tissue (framed in red). The experiment was done using samples pooled from three different animals (n = 3 animals per group).

(Fig. 3). Seventy-three putative *N*-glycans were detected between the samples analysed (Supplemental Table 2), showing an overall predominance of complex-type structures over high mannose and hybrid type, independently of the developmental stage (Fig. 3 A). Specifically, the relative percentage of complex-type *N*-linked glycans increased from three-day-old to adult samples (56% and 61%, respectively) (Fig. 3 B). Consequently, the amount of high mannose-type *N*-glycans decreased from 37% at early neonatal stage to 31% at the adult stage (Fig. 3 B). Remaining hybrid-type structures was found to be 7% in neonatal and 8% in adult (Fig. 3 B). However, the adult tended to have a shorter form of hybrid-type, whereas the neonatal tended to have a more sialylated (larger) form of hybrid-type. In the data analysed, the predominant high mannose structure was $Hex_9HexNAc_2$ (Man9) in both neonatal

and adult samples (Fig. 3 C). Among all the high mannose structures quantified, the difference between the groups did not exceed 2%, apart from $Hex_6HexNAc_2$ (Man6) that decreased from 7% in neonatal to 2% in adult (Fig. 3 C).

The adult tissue had higher expression of sialylated *N*-glycans (64%) but slightly lower core fucosylation (44%) than that of neonatal (57% and 47%, respectively), whereas the α-(2,6)-linked Neu5Ac level was similar (30%) in both samples. In addition, *N*-linked glycans with disialic acid terminus (Neu5Ac-α-(2,8)-Neu5Ac) in adult rat (10%) were higher than that in neonatal (1%). As shown in Fig. 3, $Neu5Ac_4Hex_6HexNAc_5deHex_1$ (*m/z 1658*, di-sialylated) and $Neu5Ac_2Hex_5HexNAc_4$ (*m/z* 1111, without core fucosylation) were higher in adult stage (6% and 9%) than in the neonatal one (1% and 2%), whereas $Neu5Ac_2Hex_5HexNAc_4deHex_1$ (*m/z* 1184, core fucosylated) showed a higher expression in neonatal (19%) than in the fully developed stage (13%). *N*-glycans containing terminal Gal-α-(1,3)-Gal disaccharides were similar between neonatal condition (9%) and adult stage (8%). As illustrated in Fig. 4 A, one complex-type, containing terminal α-galactose (Gal-α-(1,3)-Gal-β-(1,4)-GlcNAc-β-(1,2)-Man-α-(1,3)-[Gal-α-(1–3)-Gal-β-(1,4)-GlcNAc-β-(1,2)-Man-α-(1,6)-]Man-β-(1,4)-GlcNAc-β-(1,4)-GlcNAcol, with [M-H] ion of *m/z* 1965 in Supplemental Table 2), one high mannose-type (Glc-α-(1,3)-Man-α-(1,2)-Man-α-(1,2)-Man-α-(1,3)[Man-α-(1,2)-Man-α-(1,3)-Man-α-(1,2)-Man-α-(1,6)-Man-α-(1,6)]Man-β-(1,4)-GlcNAc-β-(1,4)-GlcNAcol, with [M-H] ion of *m/z* 2045 in Supplemental Table 2) and one hybrid-type (GlcNAc-β-(1,2)-Man-α-(1,3)-[Man-α-(1,2)-Man-α-(1,3)Man-α-(1,2)-Man-α-(1,6)-Man-α-(1,6)-]Man-β-(1,4)-GlcNAc-β-(1,4)-GlcNAcol, with [M-H] ion of *m/z* 1762–1 in Supplemental Table 2) putative structures were detected in the three-day-old group, all having relative percentages around 1%.

O-linked glycan analysis of neonatal and adult myocardium

O-glycome analysis revealed core 1 and 2 type *O*-glycans. A total of 15 *O*-glycans were identified across the samples analysed and most of these were sialylated (>90%) with either Neu5Ac or Neu5Gc (Supplemental Table 3). Neither core 1 nor 2 *O*-glycans were found to be elongated with oligoLacNAc extension, probably due to high sialylation (≥90%). In adult, the level of core 2 *O*-glycans was about 42%, while in neonatal the level was about 47%; on the other hand, core 1 *O*-glycans were similar between the two samples. Interestingly, a sulfated core 2 *O*-glycan ([M-H]-ion of *m/z* 1120, Supplemental Table 3) was detected in neonatal tissue (7%), as shown in Fig. 4 B. In addition, core 3 (GlcNAc-β(1,3)-GalNAcol) and sialyl-Tn (NeuAc-α-(2,6)-GalNAcol) structures had higher abundances in adult tissue than in neonatal (with [M-H]-ions of *m/z* 425 and 513, respectively, in Supplemental Table 3). Neither ABO nor Lewis type antigens were detected in either of the samples.

Distinct tissue glycosylation between neonatal and adult myocardium

Early neonatal (three-day-old), later stage (14-day-old) and fully adult (eight-month-old) left ventricular tissues of Sprague-Dawley healthy rats were analysed by lectin microarray to confirm the variations in glycosylation elucidated by LC-MS/MS (Fig. 5 A). Three profiles of the membrane glycans indicated binding to most of the same lectins that were described in the comparison between adult ventricles, although significantly different binding intensities suggested a different expression of certain glycan subgroups. A heat map showing all the relative binding intensities to the lectins tested is shown in Fig. 5 B. The presence of high mannose glycans was suggested by binding to Lch-B, Calsepa, NPA, GNA and ConA lectins (Supplemental Table 1). Glycans containing sialic acids binding to TJA isolectin I, MAA, SNA and WGA lectins were detected. Moreover in adult ventricles, high binding to RCA-I/120 lectin and PHA-E suggested that Gal-β-(1,4)-GlcNAc and bisecting GlcNAc,β-Gal/Gal-β-(1,4-)GlcNAc were present among the complex type glycans. Similarly, terminal α-galactose was expressed also at the neonatal stages, as evidenced by the binding to MPA, MOA and GS-I-B4 (Supplemental Table 1).

Hierarchical clustering of the lectin microarray binding intensity data showed an 80% similarity across all the samples profiled with the exception of one adult individual which had a similarity of 68% with the rest of the samples, and may have represented an outlier (Fig. 5 B). Interestingly, three-day-old neonatal individuals showed an 88% similarity and clustered together, showing the highest similarity inside the same group. Groups of samples belonging to the 14-day-old stage and fully adult were clustered in a dispersed way; thus the individual variability inside each of those groups was higher than any distinct difference between the later stage neonatal and adult groups (Fig. 5 B). One-way ANOVA analysis validated the trend in increased complex *N*-glycans seen by LC-ESI-MS/MS (Fig. 5 C). Specifically, a higher binding to TJA-I, *Solanum tuberosum* (STA), WGA, *Cicer arietinum* (CPA) and *Lotus tetragonolobus* (LTA) lectins (Supplemental Table 1) indicated residues which can be present in complex *N*-glycans, such as α-(2,6)-linked sialic acid, GlcNAc, sialic acid, complex glycopeptides and α-(1,2/3)-linked fucose, respectively (Fig. 5 C). Moreover, an increased binding to *Glycine max* (SBA), *Agaricus bisporus* (ABL) and *Arachis hypogaea* (PNA) lectins (Supplemental Table 1) validated the increase of *O*-glycan core 1 residues (GalNAc and Gal-β-(1,3)-

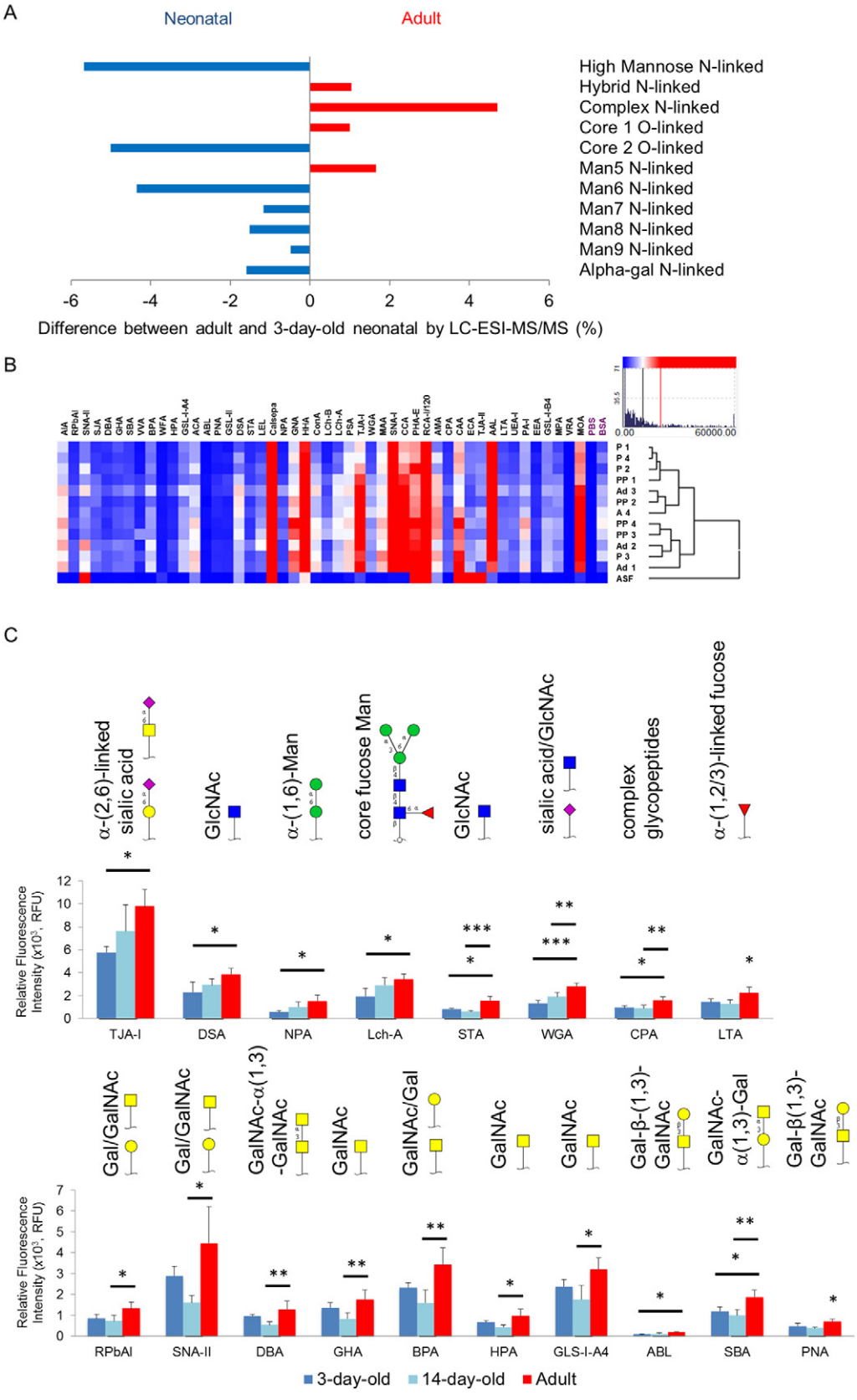

Fig. 5 (*legend on next page*)

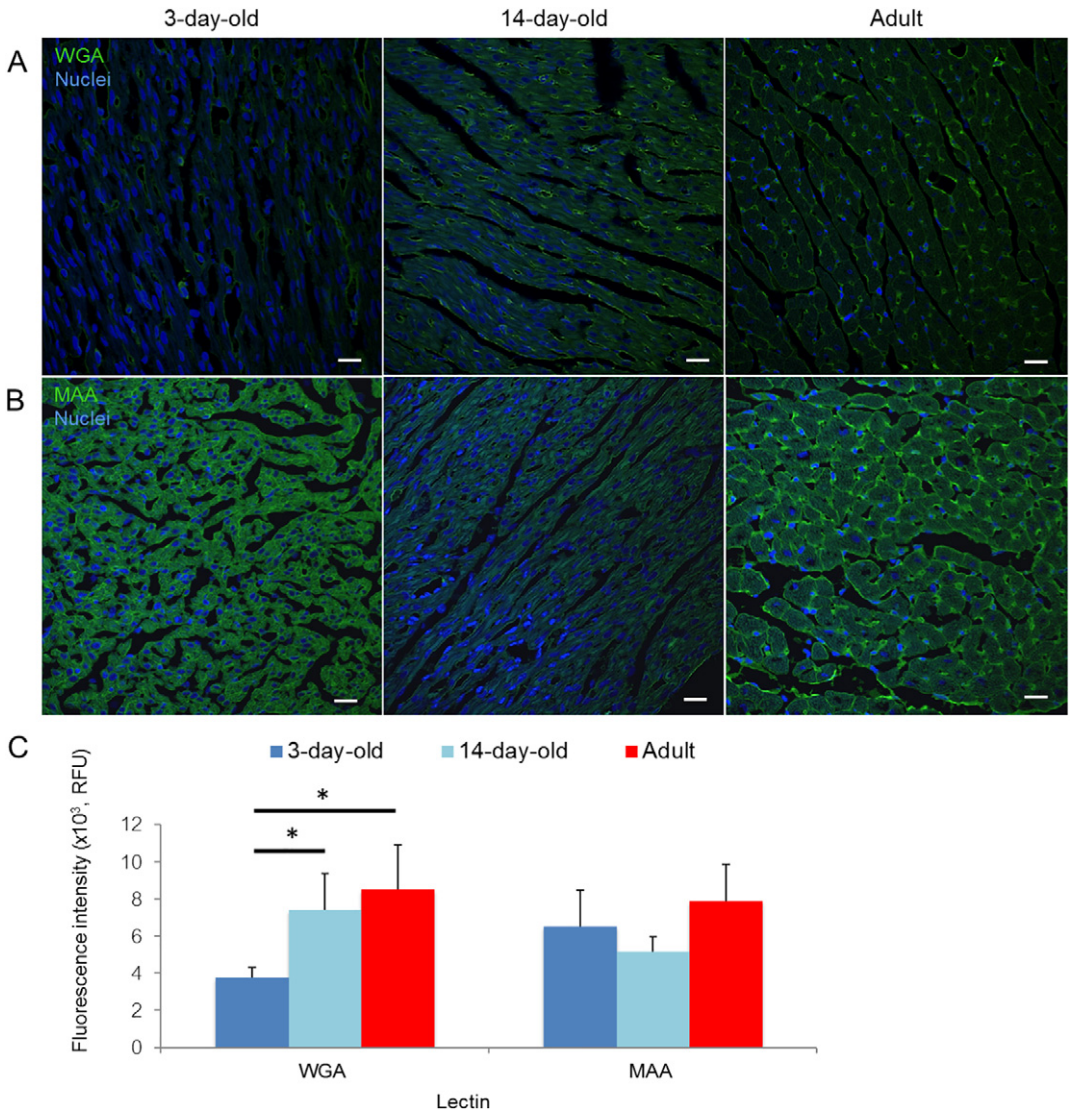

Fig. 6. Lectin histochemistry in neonatal and adult left ventricle and relative quantification. Representative images of WGA and MAA lectin histochemistry to support lectin microarray results. WGA binds to sialic acid and GlcNAc residues (A), MAA recognizes α-(2,3)-linked sialic acid (B). All lectin binding intensities were background-subtracted and quantified by Image J (C). One-way ANOVA with Tukey's post hoc correction confirmed a higher binding of WGA to adult sample. Data are shown as mean with standard deviation (n = 3–4 animals per group). * denotes significant differences between the different groups at $p < 0.05$. Scale bar = 20 μm.

Fig. 5. Higher complex *N*-glycans and lower core 1 *O*-glycans at early neonatal stage. (A) LC-ESI-MS/MS analysis showed trends of higher expression of complex *N*-glycans and lower core 2 *O*-glycans in adult left ventricular myocardial tissue from Sprague Dawley healthy rats. (B) Lectin microarrays indicated the binding intensity to the glycans present in the membrane proteins extracted from three-day-old neonatal (P), 14-day-old neonatal (PP) and adult (Ad). Hierarchical clustering showed an 80% similarity across all the samples tested with the exception of Ad1, which had a 68% similarity with the rest of the samples. Three-day-old neonatal samples P1, P2 and P4 showed an 88% similarity and clustered together, having the highest similarity inside the same group. Asialofetuin (ASF) was used as a control glycoprotein and all lectin binding intensities were normalized. All 90% laser scan measurements recorded were below the saturation limit (60,000 RFU). (C) One-way ANOVA with Tukey's post hoc correction confirmed a higher binding of lectins to complex *N*-glycans (TJA-I, DSA, NPA, upper graphs), and core 1 *O*-glycans (lower graphs). * denotes significant differences between the different groups at $p < 0.05$, ** if $p < 0.01$, *** if $p < 0.001$ (n = 4 animals per group). The experiment was carried out in technical triplicate.

GalNAc) in adult, a rise which was barely seen from the *O*-glycome. In addition, a whole different ANOVA cluster showed a higher binding intensity in the adult group than that in the 14-day-old and it was composed by GalNAc-binding lectins RPbAI, SNA-II, *Dolichos biflorus* (DBA), *Glechoma hederacea* (GHA), *Bauhinia purpurea* (BPA), *Helix pomatia* (HPA) and GSL-I-A4 (Supplemental Table 1). Finally, the increase in fucosylation seen in neonatal *N*-glycans was reflected in an increased - although non-significant - binding to *Aleuria aurantia* (AAL) lectin (Supplemental Fig. 1). A non-significant trend of higher expression of complex N-glycans was seen in the 14-day-old group than the early neonatal one, and the groups of lectins listed above confirmed the different glycosylation between the three-day-old and the adult stage indicated by clustering analysis (Fig. 5 C). Moreover, lectin histochemistry was performed to further support the lectin microarray results (Fig. 6). Higher binding to WGA was seen in adult than in early neonatal stage (Fig. 6 A,C). Consistently with the microarrays, non-significant differences such as the binding to MAA were confirmed (Fig. 6 B,C).

Discussion

Cardiac regenerative potential is present in mammals only at the early neonatal stage [1,2], and the rapid loss of this capability is a well-known limitation of this type of tissue after the occurrence of tissue damage. Due to the importance of glycosylation in the regulation of the cellular microenvironment through interactions of the cell glycocalyx and the ECM, identifying glycosylation-related mechanisms associated with pathological degeneration could provide key targets for novel therapeutic strategies [17,18]. Moreover, recently glycosylation differences of ECM and cells related to ageing were characterized [9], and in the cardiac field a precise correlation was found between the alterations in the structure and function of heparan sulfate and the physiological decline of growth factor recruitment in the ECM [13].

Studies to characterize the glycosylation of the myocardial and skeletal muscle tissues have been mainly histologically-based using lectins to indicate the presence of different types of glycosylation [19–22]. Most of these studies differentiated for cytosolic or membrane localisation in the tissue of interest. Our work not only localised the binding of a panel of biologically-relevant lectins to rat cardiomyocytes surfaces and capillaries, but assessed the consistency of the glycosylation expression across different strains of rat healthy left and right cardiac ventricles. Further, we distinguished a differential localisation of terminal sialic acids with different linkages with α-(2,6)-sialylation located on capillaries and α-(2,3)-sialylation on the cardiomyocytes membranes. SNA binding to capillaries but not cardiomyocytes was likely to be as a result of the lack of α-(2,6)-sialic acids on the cell surface, consistent with what was previously reported [20]. From a ligand-receptor perspective, the consistent expression of α-(2,6)-sialic acids on surfaces of vessels could be a mechanism to regulate the receptors implicated with angiogenesis, such as vascular endothelial growth factor receptor (VEGFR), hepatocyte growth factor receptor (HGFR) and epidermal growth factor-related ERBB receptor [16]. Recently, a high abundance of this linkage of sialic acid was assessed also in vessels characterizing anti-VEGF sensitive tumours [23] and the knockdown of α-(2,6)-sialyltransferase (ST6Gal-I) significantly reduced the motility of colon cancer cells [24].

The consistent expression of GlcNAc residues on the cardiomyocytes surfaces reflects previous findings [19,25] and indicates the relevance of this glycan in the composition of the glycocalyx which characterizes the cellular membrane. Binding to DSA lectin was seen both by lectin histochemistry and microarrays, and indeed their binding residues GlcNAc-β-(1,4)-linked and Gal-β-(1-4)-GlcNAc were detected also in the N-glycans structures by LC-MS/MS. Nevertheless, there were not relevant differences associated with the expression of these residues in our maturation comparison.

The main limitation of the results hereby presented stems from the variability of strains of rat and genders which were used for the initial determination of a healthy adult baseline, whereas the same strain was used for the final ageing comparison. Rat myocardial left ventricle tissues from two post-neonatal stages (three- and 14-day-old) had consistent glycosylation and both differed from adult glycosylation. After the recent advances in the development of LC-ESI-MS/MS to quantify *N*- and *O*-glycans [26–28], it was possible to see for the first time in this study a higher expression of complex glycans on the cellular membrane and ECM in the adult stage than in the early neonatal, including di-sialylated *N*-glycans (NeuAc-α(2-8)-NeuAc). The higher expression of complex-type structures correlates with the lectin microarray, in particular in the binding to WGA, CPA and LTA lectins. A higher binding to WGA reflected the increased sialylation in adult detected in *N*-glycans by LC-MS/MS. Previous studies have established the importance of both *N*- and *O*-linked glycans in voltage gated ion channel activity which is fundamental for heart cells contractility [29,30]. Specifically, enzymatic desialylation experiments were performed to demonstrate the modulation of the functioning of voltage-gated potassium channels by *N*- and *O*-glycans [30,31], and the relevance of polysialic acid was highlighted on the conductive properties of cardiac cells. Deletion of polysialyltransferase ST8sia2 enzyme significantly affected the action potential of sodium channels in

atrial cardiomyocytes whereas this did not occur with ventricular cardiomyocytes [29]. In our study, the higher expression of NeuAc-α(2-8)-NeuAc detected in the adult compared to the neonatal ventricular whole membrane and ECM lysate could instead reflect the role of polysialic acid in the regulation of cell-ECM. This specific structure has been studied for the potential activation of fibroblast growth factor signalling by its expression on neural cell adhesion molecules (NCAM) [16,32].

N-linked glycan analysis showed a 5% increase in the portion of complex-type structures and a 6% decrease in the subgroup of high mannose structures in adult compared to three-day-old neonatal. Interestingly, the results of the LC-MS/MS analysis performed in this study identified a 4% increase in relative percentage of the $Man_6GlcNAc_2$-structure in neonatal cardiac tissue. The greater expression of this high mannose type structure in neonatal tissue may be an indication of stemness of the tissue, as high percentages of high mannose structures were detected in total protein lysates of pluripotent stem cells [33,34]. Thereby, the increase in surface expression of high mannose structures may be due to the temporary expansion of the endoplasmic reticulum which is needed for the translational processes more than a sign of cellular stress [35,36].

Moreover, in this study we identified three specific *N*-glycan structures that were present in the neonatal tissue. Among these structures, a complex-type structure with terminal Gal-α-(1,3)-Gal disaccharide ([M-H] ion of *m/z* 1965) and a high mannose type structure, $Hex_{10}HexNAc_2$ (Glc_1Man_9) ([M-H]-ion of *m/z* 2045), were also previously not found in adult tissue [37]. The detection of $Hex_{10}HexNAc_2$ in neonatal tissue, together with increase in the abundance of $Man_6GlcNAc_2$, might indicate a different cellular-type composition at three days after birth, i.e. in the middle of the self-regenerating capability of the mammalian heart [2]. Finally, the observed decrease in high mannose-type *N*-glycans in myocardial total membranes samples upon ageing reflects the same trend seen in both differentiated cardiomyocytes and fibroblasts when compared to induced pluripotent stem cells (iPSCs) [34,38]. Nevertheless, the distinctive increase in the relative abundance of $Man_5GlcNAc_2$- in iPSCs [34] was not seen in the neonatal total membranes, whereas $Man_6GlcNAc_2$- and $Man_{10}GlcNAc_2$- accounted for the higher abundance in total high mannose retained at the early neonatal stage (three days after birth). Consistently with these findings relative to high mannose-type *N*-glycans, the stemness of three-day-old neonatal tissue was highlighted also by two additional observations in our study. First, the reported decrease in sialylated *N*-glycans in neonatal was reported also when comparing differentiated cardiomyocytes to stem cells [38]. Second, the increase in core fucosylation seen both in *N*-linked glycans correlated with its already reported distinctive presence in undifferentiated (iPSCs) rather than in the somatic state (fibroblasts) [34].

Further, to the best of our knowledge, this work is the first structural analysis of *O*-linked glycans in rat cardiac tissue, either neonatal or adult. Interestingly, in both neonatal and adult, unlike *O*-glycans containing both Neu5Ac and Neu5Gc, all detected sialylated *N*-glycans contained only Neu5Ac. This finding could be apparently in contrast with the previously reported expression of Neu5Gc in the total lysate of cardiomyocytes and ventricular/atrial tissue [29,34], but the samples analysed in this study were membrane proteins. Therefore, the accumulation of *N*-linked glycans containing NeuGc in the intracellular portion as a result of a metabolic pathway might account for this difference [39]. On the other hand, the retention of Neu5Gc on the epithelial cells whose glycocalyx contain *O*-linked glycans could justify why they were detected in both neonatal and adult. Interestingly, a sulfated core 2 *O*-glycan structure (Neu5Ac-α-(2,3)-Gal-β-(1,3)-[(3S)Gal-β-(1,4)-GlcNAc-β-(1,6)-]GalNAc-ol) was detected in the 3-day-old neonatal sample. This is a carbohydrate determinant present on the glycoproteins coating endothelial mucins such as CD34 [40] which is expressed during early vasculogenesis, angiogenesis and hematopoiesis [41].

In conclusion, these results show glycosylation in different stages of healthy myocardial tissue. Consistent glycosylation was shown across the left ventricular tissue and demonstrated to be similar to the right ventricle. Moreover, we showed that rat maturation is associated with precise changes in *N*- and *O*-linked glycan structures which were screened by LC-ESI-MS/MS and validated by lectin microarray analysis. These findings represent a well-characterized basis of comparison for the investigation of glycosylation changes in the myocardial tissue in a pathological scenario such as ischemia or cardiac pressure overload. With the identification of potential glycan targets in this work, the future glycan-targeted therapies might be designed to enhance an ECM-inspired restoration of the myocardial tissue following myocardial infarction.

Experimental procedures

Tissue harvesting from adult and neonatal rats

All adult and neonatal rats were carcasses which were kindly made available for harvesting from National University of Ireland Galway according to the EU Directive 2010/63. None of the animals were subjected to any procedure which could potentially affect their circulatory system before sacrifice. Specifically, three-month-old adult male Lewis and seven-month-old female Dark Agouti rats (n = 6 animals per

group) were used to assess the glycoprofile of left ventricles between different strains. Secondly, three seven-month-old adult male Lewis and three seven-month-old adult male Fischer rats (n = 3 animals per group) were used to check for differences between left and right ventricle of the heart. Finally, three-day-old neonatal female, 14-day-old neonatal female and six-month-old adult female rats, all belonging to the Sprague Dawley strain (n = 4 animals per group), were used for the different ageing stage comparison. Each animal was wiped with 70% ethanol at the thorax where an incision was made to remove the skin layer and then the sternum was cut to gain access to the internal organs. The heart was excised by cutting the great vessels and each heart was immediately placed in Hank's balanced salt solution (HBSS) and washed to remove the excess of blood. The remaining great blood vessels and atria were then removed using a fine blade and the heart was positioned in a cross-section orientation to clearly distinguish the left ventricle thick wall, the interventricular septum and the collapsed thin right ventricle.

Tissue processing and cryosectioning

Tissue samples having a thickness of approximately 0.3 cm from left and right ventricles of adult Lewis and Fischer hearts and from the left ventricle of neonatal and adult Sprague Dawley hearts were immediately excised after harvesting, washed briefly in HBSS and snap-frozen for later protein extraction.

Left ventricle heart tissues from adult Lewis and Dark Agouti rats were fixed on freshly prepared 4% paraformaldehyde (PFA) in PBS overnight at 4 °C. Tissues were then washed with HBSS, infiltrated in freshly prepared sterile-filtered 30% sucrose solution overnight at 4 °C, embedded in optimal cutting temperature compound (OCT) medium (Sakura Finetek, Torrance, CA, USA) and stored at –80 °C. Embedded tissue was cut into 5 µm tissue sections using a cryostat (Leica CM1850, Wetzlar, Germany) at –20 °C and tissue was placed flat immediately on Superfrost™ microscope slides (Thermo Fisher Scientific, Waltham, MA, USA). Intact tissue slides were stored at –80 °C until use.

Lectin histochemistry

Fixed cryosections from healthy Lewis and Dark Agouti left ventricles were washed twice for 3 min each with Tris-buffered saline (TBS; 20 mM Tris-HCl, 100 mM NaCl, 1 mM, $CaCl_2$, 1 mM $MgCl_2$, pH 7.2) with 0.05% Tween-20 (TBS-T) and then once in TBS. Tissue sections were then blocked with 2% periodate-treated bovine serum albumin (BSA) [42] in TBS for 1 h at room temperature (RT), washed once in TBS and then incubated with a single fluorescein isothiocyanate- (FITC-)labelled lectin (listed in Table 1) diluted in TBS for 1 h at RT. Five lectins with various carbohydrate-binding specificities (DSA, SNA-I, MAA, WGA and ConA) were incubated with tissues. All incubations including and subsequent to labelled lectin incubations were carried out in the dark and slides were always protected from light. To verify carbohydrate-mediated binding [43], lectins were also co-incubated with their respective haptenic sugars for 1 h before incubating the mixture on the tissue sections. After lectin incubation, sections were washed three times with TBS and then coverslipped with ProLong® Gold antifade with DAPI (Thermo Fisher Scientific, Waltham, MA, USA). The slides were cured at 4 °C in the dark for 1 day before imaging. Tissues were imaged using an inverted epifluorescence microscope (Olympus IX81, Olympus, Tokyo, Japan). Seven to nine images per section of each tissue sample were taken at 20× magnification. Images from lectin histochemistry using WGA and ConA lectins were taken at 40× and 60× magnification, respectively. To support the lectin microarray experiment comparing neonatal and adult cellular membrane protein samples, lectin histochemistry was performed as described above on sections from four 3-day-old, four 14-day-old and three adult Sprague Dawley rats. A grid was superimposed on each image to quantify fluorescence intensity using Image-J after background correction.

Protein extraction and quantification

Cytosolic and membrane protein fractions were extracted from left and right ventricles of the adult Lewis and Fischer hearts and from the left ventricle of neonatal and adult Sprague Dawley hearts using the Mem-PER™ Plus Membrane Protein Extraction Kit (Thermo Fisher Scientific, Waltham, MA, USA). Tissue samples (approximately 50 mg each) were washed in Cell Wash Solution and mixed for 30 s. The tissue was then cut finely into smaller pieces with scissors, placed in a 2 ml tissue grinder and 1 ml permeabilization buffer with 1× cOmplete™ EDTA-free protease inhibitor cocktail (Roche, Basel, Switzerland) was added. The tissue was homogenized manually at RT until a uniform suspension was obtained and the suspension was incubated for 10 min at 4 °C. The homogenate was then centrifuged (16,000 ×g, 15 min, 4 °C and the supernatant (cytosolic fraction) was aliquoted and stored at –80 °C. The pellet (membrane fraction) was resuspended with Solubilisation buffer (with protease inhibitor cocktail) until a homogenous suspension was obtained and incubated for 30 min at 4 °C with shaking. The membrane fraction was centrifuged again as above and the supernatant containing the membrane proteins was aliquoted and stored at 4 °C. Protein content was quantified using a Micro BCA™ Protein Assay Kit (Thermo Fisher Scientific, Waltham, MA, USA) by comparison to a BSA standard.

Fluorescent labelling of membrane proteins

Membrane protein samples extracted as detailed in the previous paragraph from left and right ventricles of the adult Lewis and Fischer hearts and from the left ventricle of neonatal and adult Sprague Dawley hearts were thawed on ice and diluted to approximately 2 mg/ml in 100 mM sodium bicarbonate, pH 8.2, (approximately 250 µl final volume per sample). Approximately 50 µg of Alexa Fluor® 555 Succinimidyl Ester (Thermo Fisher Scientific, Waltham, MA, USA) dissolved in dry dimethyl sulfoxide was added to each protein sample and incubated for 2 h at RT with gentle shaking and always protected from light. Labelled samples were filtered through 3 kDa molecular weight cut-off (MWCO) centrifugal filters (Amicon®, Millipore, Burlington, MA, USA) and buffer-exchanged in PBS supplemented with 1× cOmplete™ EDTA-free protease inhibitor cocktail (Roche, Basel, Switzerland). Absorbance at 280 and 555 nm was measured for each sample and protein concentration and labelling substitution was calculated for each sample according to manufacturer's instructions using and arbitrary E of 10 and molecular mass of 100 kDa for the protein mixtures to facilitate relative quantification between samples [44]. Labelled protein samples were stored at –80 °C until use.

Lectin microarray analysis

Lectin microarrays were printed using a library of 48 lectins with varying specificities for different carbohydrate structures (Supplemental Table 1) as previously described [45]. Fluorescently labelled membrane proteins were incubated on lectin microarrays essentially as previously described [44] with limited light exposure throughout the process. Initially, a titration of labelled protein from 1 to 10 µg/ml was incubated to determine the optimal concentration for all samples to obtain an extractable, non-saturated signal response (i.e. >1000 and <65,000 relative fluorescence units (RFU)) with low background (<500 RFU) for all samples. For incubations, all labelled membrane protein samples were thawed on ice and diluted to 2.5 µg/ml in TBS-T. After incubation, washing and drying, microarray slides were scanned immediately using a G2505 microarray scanner (Agilent Technologies, Santa Clara, CA, USA) using a 532 nm laser (5 µm resolution, 90% laser power). Each sample was individually incubated on three different microarray slides for three technical replicate experiments.

Resulting image files (.tif) were extracted essentially as previously described [44] using GenePix Pro v6.1.0.4 software (Molecular Devices, Wokingham, UK). Local background-corrected median feature intensity data were analysed and the median of six replicate spots per subarray was handled as a single data point for graphical and statistical analysis. Data was normalized to the per-subarray (i.e. per sample) total intensity mean across three replicate experiments. Binding data was presented as bar charts of average intensity with one standard deviation of three experimental replicates. Clustering of the normalized data was done using Hierarchical Clustering Explorer v3.5 (HCE 3.5, University of Maryland, http://www.cs.umd.edu/hcil/hce/hce3.html) using Euclidean distance with complete linkage.

Release of *N*- and *O*-linked glycans from membrane proteins

Membrane protein samples from adult and neonatal Sprague-Dawley healthy rats (240 µg) were pooled from three different animals per group. Extraction buffer was exchanged to 7 M urea via 30 kDa MWCO centrifugal filter (Millipore, Burlington, MA, USA) and incubated with 25 mM dithiothreitol at 56 °C for 45 min. The reduced samples were then alkylated with 62.5 mM iodoacetamide at RT for 50 min in the dark. After alkylation, samples were treated with sequencing grade trypsin (1% w/w, Promega, Madison, WI, USA) at 37 °C overnight. Tryptic peptides were precipitated with 80% (v/v) acetone. The dried pellet was then washed twice with 500 µl of cold 60% methanol and pellets were air-dried. After adding 50 µl of 50 mM ammonium bicarbonate, pH 8.4, and 1 µl of PNGase F (Asparia Glycomics, Donostia-San Sebastián, Spain), samples were incubated at 37 °C overnight.

Released *N*-linked glycans were separated from (*O*-glyco)peptides using a SEP-Pak C18 cartridge (Waters Corporation, Milford, MA, USA). Briefly, the cartridge was first conditioned with different dilutions (90% and 10%) of acetonitrile (ACN) in 0.5% trifluoroacetic acid (TFA). After applying the sample, both the eluent and washout with 5% acetic acid were combined which contained released *N*-linked glycans. *O*-glycopeptides were eluted by the addition of 65% ACN in 0.5% TFA. Both samples were then dried at 30 °C. Released *N*-linked glycans were reduced by 0.5 M sodium borohydride ($NaBH_4$) and 20 mM NaOH at 50 °C overnight. *O*-linked glycans were released by the reductive β-elimination reaction. Briefly, samples were incubated in a buffer containing 0.5 M $NaBH_4$ and 50 mM NaOH at 50 °C overnight. Reactions were quenched with glacial acetic acid, and samples were desalted and dried as previously described [46].

LC-ESI-MS/MS analysis

Released glycans were dissolved in deionized water and analysed by liquid chromatography-electrospray ionization tandem mass spectrometry (LC-ESI/MS) as previously reported [47]. The oligosaccharides were separated on a column (10 cm × 250 µm) packed in-house with 5 µm porous graphite particles (Hypercarb™, Thermo Fisher Scientific, Waltham, MA, USA). The oligosaccharides

were injected on to the column and eluted with an ACN gradient (Buffer A, 10 mM ammonium bicarbonate; Buffer B, 10 mM ammonium bicarbonate in 80% ACN). The gradient (0–45% Buffer B) was eluted for 46 min, followed by a wash step with 100% Buffer B, and equilibrated with Buffer A in the following 24 min. A 40 cm × 50 μm i.d. fused silica capillary was used as transfer line to the ion source.

The samples were analysed in negative ion mode on a LTQ linear ion trap mass spectrometer (Thermo Fisher Scientific, Waltham, MA, USA), with an IonMax standard ESI source equipped with a stainless steel needle kept at –3.5 kV. Compressed air was used as nebulizer gas. The heated capillary was kept at 270 °C, and the capillary voltage was –50 kV. Full scan (*m/z* 380–2000 two microscans, maximum 100 ms, target value of 30,000) was performed, followed by data-dependent MS^2 scans (two microscans, maximum 100 ms, target value of 10,000) with normalized collision energy of 35%, isolation window of 1.0 units, activation q = 0.25 and activation time 30 ms). The threshold for MS^2 was set to 300 counts. Data acquisition and processing were conducted with Xcalibur™ software (Version 2.0.7, Thermo Fisher Scientific, Waltham, MA, USA).

Glycan structures were identified from their MS/MS spectra by manual annotation. For structural annotation, some assumptions were made in this study. The structures of *N*- and *O*-linked glycans were assumed to follow the classic biosynthetic pathways. Diagnostic fragmentation ions for *N*- and *O*-glycans were investigated as previously described [48]. Terminal hexose units (Hex2) were presumed to be α-linked Gal. Chain elongation was expected to be mediated by the addition of *N*-acetyllactosamine (LacNAc) disaccharides. The annotated structures were submitted to the UniCarb-DR database (http://unicarb-dr.biomedicine.gu.se/references/351) according to MIRAGE guidelines [49] and will be included in the next release. For comparison of glycan abundances between samples, individual structures were quantified relative to the total content by integration of the extracted ion chromatogram peak area. The area under the curve (AUC) of each structure was normalized to the total AUC and expressed as a percentage. The peak area was processed by Progenesis QI (Nonlinear Dynamics Ltd., Newcastle upon Tyne, UK).

Statistical analysis

All statistical analysis was performed using Minitab Express™ software (Minitab, Inc. State College, PA, USA). Lectin histochemistry data were selected by significance as assessed by standard Student's *t*-test and by one-way ANOVA with Tukey's post-hoc correction, depending on the number of groups. Lectin microarray data analysis was compared using one-way ANOVA with Tukey's post-hoc correction. Values were considered significant with $p < 0.05$.

Acknowledgments

The authors would like to thank Dr. Oliver Treacy, Dr. Paul Lohan and Mr. Vaibhav Patil from National University of Ireland Galway for having kindly made available for harvesting hearts from carcasses of adult and neonatal rats. In addition, the authors would like to acknowledge Mr. Anthony Sloan for editorial assistance and Mr. Maciej Doczyk for assistance in drawing the schematics presented in this article.

Funding

This work was supported by the European Union funding under the AngioMatTrain 7th Framework Programme, Grant Agreement Number 317304 and the research grant from Science Foundation Ireland (SFI) co-funded under the European Regional Development Fund under Grant Number 13/RC/2073. This work was also supported by the Naughton Foundation, NSF-CBET CAREER Award # 1651385 and NSF CBET Award # 1805157. MS analysis of glycans was performed by the Swedish infrastructure for biological mass spectrometry (BioMS) supported by the Swedish Research Council. The authors acknowledge the use of the facilities of the Centre for Microscopy and Imaging at the National University of Ireland Galway, a facility that is co-funded by the Irish Government's Programme for Research in Third Level Institutions, Cycles 4 and 5, National Development Plan 2007–2013.

Appendix A. Supplementary data

Supplementary data to this article can be found online at https://doi.org/10.1016/j.matbio.2019.05.001.

Received 29 January 2019;
Received in revised form 18 April 2019;
Accepted 14 May 2019
Available online 17 May 2019

Keywords:
Heart regeneration;
Glycobiology;
Lectin microarrays;
Glycomics;
Neonatal

References

[1] L. Ye, G. D'Agostino, S.J. Loo, C.X. Wang, L.P. Su, S.H. Tan, G.Z. Tee, C.J. Pua, E.M. Pena, R.B. Cheng, W.C. Chen, D. Abdurrachim, J. Lalic, R.S. Tan, T.H. Lee, J. Zhang, S.A.

Cook, Early regenerative capacity in the porcine heart, Circulation 138 (24) (2018) 2798–2808.
[2] E.R. Porrello, A.I. Mahmoud, E. Simpson, J.A. Hill, J.A. Richardson, E.N. Olson, H.A. Sadek, Transient regenerative potential of the neonatal mouse heart, Science 331 (6020) (2011) 1078–1080.
[3] W. Zhu, E. Zhang, M. Zhao, Z. Chong, C. Fan, Y. Tang, J.D. Hunter, A.V. Borovjagin, G.P. Walcott, J.Y. Chen, G. Qin, J. Zhang, Regenerative potential of neonatal porcine hearts, Circulation 138 (24) (2018) 2809–2816.
[4] X. Wang, T. Ha, L. Liu, Y. Hu, R. Kao, J. Kalbfleisch, D. Williams, C. Li, TLR3 mediates repair and regeneration of damaged neonatal heart through glycolysis dependent YAP1 regulated miR-152 expression, Cell Death Differ. 25 (5) (2018) 966–982.
[5] M. Notari, A. Ventura-Rubio, S.J. Bedford-Guaus, I. Jorba, L. Mulero, D. Navajas, M. Martí, Á. Raya, The local microenvironment limits the regenerative potential of the mouse neonatal heart, Sci. Adv. 4 (5) (2018) eaao5553.
[6] B. Greenberg, J. Butler, G.M. Felker, P. Ponikowski, A.A. Voors, A.S. Desai, D. Barnard, A. Bouchard, B. Jaski, A.R. Lyon, J.M. Pogoda, J.J. Rudy, K.M. Zsebo, Calcium upregulation by percutaneous administration of gene therapy in patients with cardiac disease (CUPID 2): a randomised, multinational, double-blind, placebo-controlled, phase 2b trial, Lancet 387 (10024) (2016) 1178–1186.
[7] S.V. Rao, U. Zeymer, P.S. Douglas, H. Al-Khalidi, J.A. White, J. Liu, H. Levy, V. Guetta, C.M. Gibson, J.F. Tanguay, P. Vermeersch, J. Roncalli, J.D. Kasprzak, T.D. Henry, N. Frey, O. Kracoff, J.H. Traverse, D.P. Chew, J. Lopez-Sendon, R. Heyrman, M.W. Krucoff, Bioabsorbable intracoronary matrix for prevention of ventricular remodeling after myocardial infarction, J. Am. Coll. Cardiol. 68 (7) (2016) 715–723.
[8] A. Varki, Biological roles of glycans, Glycobiology 27 (1) (2017) 3–49.
[9] E.C. Collin, M. Kilcoyne, S.J. White, S. Grad, M. Alini, L. Joshi, A.S. Pandit, Unique glycosignature for intervertebral disc and articular cartilage cells and tissues in immaturity and maturity, Sci. Rep. 6 (2016), 23062.
[10] E.C. Collin, O. Carroll, M. Kilcoyne, M. Peroglio, E. See, D. Hendig, M. Alini, S. Grad, A. Pandit, Ageing affects chondroitin sulfates and their synthetic enzymes in the intervertebral disc, Signal Transduct. Target. Ther. 2 (2017), 17049.
[11] S.E. Zalik, E. Didier, P. Didier, I.M. Ledsham, D. Bayle, E.J. Sanders, Expression of the galactose-binding lectins during the formation of organ primordia in the chick embryo, Int. J. Dev. Biol. 38 (1) (1994) 55–68.
[12] H. Hu, K. Eggers, W. Chen, M. Garshasbi, M.M. Motazacker, K. Wrogemann, K. Kahrizi, A. Tzschach, M. Hosseini, I. Bahman, T. Hucho, M. Mühlenhoff, R. Gerardy-Schahn, H. Najmabadi, H.H. Ropers, A.W. Kuss, ST3GAL3 mutations impair the development of higher cognitive functions, Am. J. Hum. Genet. 89 (3) (2011) 407–414.
[13] M.B. Huynh, C. Morin, G. Carpentier, S. Garcia-Filipe, S. Talhas-Perret, V. Barbier Chassefière, T.H. van Kuppevelt, I. Martelly, P. Albanese, D. Papy-Garcia, Age-related changes in rat myocardium involve altered capacities of glycosaminoglycans to potentiate growth factor functions and heparin sulfate-altered sulfation, J. Biol. Chem. 287 (14) (2012) 11363–11373.
[14] K. InanlooRahatloo, A.F. Parsa, K. Huse, P. Rasooli, S. Davaran, M. Platzer, M. Kramer, J.B. Fan, C. Turk, S. Amini, F. Steemers, K. Gunderson, M. Ronaghi, E. Elahi, Mutation in ST6GALNAC5 identified in family with coronary artery disease, Sci. Rep. 4 (2014) 3595.
[15] R. Péanne, P. de Lonlay, F. Foulquier, U. Kornak, D.J. Lefeber, E. Morava, B. Pérez, N. Seta, C. Thiel, E. Van Schaftingen, G. Matthijs, J. Jaeken, Congenital disorders of glycosylation (CDG): quo vadis? Eur J Med Genet. 61 (11) (2018) 643–663.
[16] I.G. Ferreira, M. Pucci, G. Venturi, N. Malagolini, M. Chiricolo, F. Dall'Olio, Glycosylation as a main regulator of growth and death factor receptors signaling, Int. J. Mol. Sci. 19 (2) (2018).
[17] I.L. Mohd Isa, S.A. Abbah, M. Kilcoyne, D. Sakai, P. Dockery, D.P. Finn, A. Pandit, Implantation of hyaluronic acid hydrogel prevents the pain phenotype in a rat model of intervertebral disc injury, Sci. Adv. 4 (4) (2018) eaaq0597.
[18] M.J. Paszek, C.C. DuFort, O. Rossier, R. Bainer, J.K. Mouw, K. Godula, J.E. Hudak, J.N. Lakins, A.C. Wijekoon, L. Cassereau, M.G. Rubashkin, M.J. Magbanua, K.S. Thorn, M.W. Davidson, H.S. Rugo, J.W. Park, D.A. Hammer, G. Giannone, C.R. Bertozzi, V.M. Weaver, The cancer glycocalyx mechanically primes integrin-mediated growth and survival, Nature 511 (7509) (2014) 319–325.
[19] A. Bardosi, L. Bardosi, M. Hendrys, B. Wosgien, H.J. Gabius, Spatial differences of endogenous lectin expression within the cellular organization of the human heart: a glycohistochemical, immunohistochemical, and glycobiochemical study, Am. J. Anat. 188 (4) (1990) 409–418.
[20] J.G. Lawrenson, J.P. Cassella, A.J. Hayes, J.A. Firth, G. Allt, Endothelial glycoconjugates: a comparative lectin study of the brain, retina and myocardium, J. Anat. 196 (2000) 55–60 Pt 1.
[21] J.S. Frank, G.A. Langer, L.M. Nudd, K. Seraydarian, The myocardial cell surface, its histochemistry, and the effect of sialic acid and calcium removal on its structure and cellular ionic exchange, Circ. Res. 41 (5) (1977) 702–714.
[22] D. Gros, B. Bruce, C.E. Challice, J. Schrevel, Ultrastructural localization of concanavalin A and wheat germ agglutinin binding sites in adult and embryonic mouse myocardium, J. Histochem. Cytochem. 30 (3) (1982) 193–200.
[23] D.O. Croci, J.P. Cerliani, T. Dalotto-Moreno, S.P. Méndez-Huergo, I.D. Mascanfroni, S. Dergan-Dylon, M.A. Toscano, J.J. Caramelo, J.J. García-Vallejo, J. Ouyang, E.A. Mesri, M. R. Junttila, C. Bais, M.A. Shipp, M. Salatino, G.A. Rabinovich, Glycosylation-dependent lectin-receptor interactions preserve angiogenesis in anti-VEGF refractory tumors, Cell 156 (4) (2014) 744–758.
[24] J. Qian, C.H. Zhu, S. Tang, A.J. Shen, J. Ai, J. Li, M.Y. Geng, J. Ding, alpha2,6-hyposialylation of c-Met abolishes cell motility of ST6Gal-I-knockdown HCT116 cells, Acta Pharmacol. Sin. 30 (7) (2009) 1039–1045.
[25] B. Emde, A. Heinen, A. Gödecke, K. Bottermann, Wheat germ agglutinin staining as a suitable method for detection and quantification of fibrosis in cardiac tissue after myocardial infarction, Eur. J. Histochem. 58 (4) (2014) 2448.
[26] P.H. Jensen, N.G. Karlsson, D. Kolarich, N.H. Packer, Structural analysis of N- and O-glycans released from glycoproteins, Nat. Protoc. 7 (7) (2012) 1299–1310.
[27] S. Yang, S. Chatterjee, J. Cipollo, The glycoproteomics-MS for studying glycosylation in cardiac hypertrophy and heart failure, Proteomics Clin. Appl. 12 (5) (2018), e1700075.
[28] D.C. Frost, L. Li, Recent advances in mass spectrometry-based glycoproteomics, Adv. Protein Chem. Struct. Biol. 95 (2014) 71–123.
[29] M.L. Montpetit, P.J. Stocker, T.A. Schwetz, J.M. Harper, S.A. Norring, L. Schaffer, S.J. North, J. Jang-Lee, T. Gilmartin,

S.R. Head, S.M. Haslam, A. Dell, J.D. Marth, E.S. Bennett, Regulated and aberrant glycosylation modulate cardiac electrical signaling, Proc. Natl. Acad. Sci. U. S. A. 106 (38) (2009) 16517–16522.
[30] T.A. Schwetz, S.A. Norring, E.S. Bennett, N-glycans modulate K(v)1.5 gating but have no effect on K(v)1.4 gating, Biochim. Biophys. Acta 1798 (3) (2010) 367–375.
[31] T.A. Schwetz, S.A. Norring, A.R. Ednie, E.S. Bennett, Sialic acids attached to O-glycans modulate voltage-gated potassium channel gating, J. Biol. Chem. 286 (6) (2011) 4123–4132.
[32] V.V. Kiselyov, V. Soroka, V. Berezin, E. Bock, Structural biology of NCAM homophilic binding and activation of FGFR, J. Neurochem. 94 (5) (2005) 1169–1179.
[33] N. Fujitani, J. Furukawa, K. Araki, T. Fujioka, Y. Takegawa, J. Piao, T. Nishioka, T. Tamura, T. Nikaido, M. Ito, Y. Nakamura, Y. Shinohara, Total cellular glycomics allows characterizing cells and streamlining the discovery process for cellular biomarkers, Proc. Natl. Acad. Sci. U. S. A. 110 (6) (2013) 2105–2110.
[34] K. Hasehira, H. Tateno, Y. Onuma, Y. Ito, M. Asashima, J. Hirabayashi, Structural and quantitative evidence for dynamic glycome shift on production of induced pluripotent stem cells, Mol. Cell. Proteomics 11 (12) (2012) 1913–1923.
[35] N. Cherepanova, S. Shrimal, R. Gilmore, N-linked glycosylation and homeostasis of the endoplasmic reticulum, Curr. Opin. Cell Biol. 41 (2016) 57–65.
[36] E. Bieberich, Synthesis, processing, and function of N-glycans in N-glycoproteins, Adv. Neurobiol. 9 (2014) 47–70.
[37] B.L. Parker, G. Palmisano, A.V. Edwards, M.Y. White, K. Engholm-Keller, A. Lee, N.E. Scott, D. Kolarich, B.D. Hambly, N.H. Packer, M.R. Larsen, S.J. Cordwell, Quantitative N-linked glycoproteomics of myocardial ischemia and reperfusion injury reveals early remodeling in the extracellular environment, Mol. Cell. Proteomics 10 (8) (2011), M110.006833.
[38] T. Kawamura, S. Miyagawa, S. Fukushima, N. Kashiyama, A. Kawamura, E. Ito, A. Saito, A. Maeda, H. Eguchi, K. Toda, S. Miyagawa, H. Okuyama, Y. Sawa, Structural changes in N-Glycans on induced pluripotent stem cells differentiating toward cardiomyocytes, Stem Cells Transl. Med. 4 (11) (2015) 1258–1264.
[39] A.K. Bergfeld, O.M. Pearce, S.L. Diaz, T. Pham, A. Varki, Metabolism of vertebrate amino sugars with N-glycolyl groups: elucidating the intracellular fate of the non-human sialic acid N-glycolylneuraminic acid, J. Biol. Chem. 287 (34) (2012) 28865–28881.
[40] G. Hernandez Mir, J. Helin, K.P. Skarp, R.D. Cummings, A. Mäkitie, R. Renkonen, A. Leppänen, Glycoforms of human endothelial CD34 that bind L-selectin carry sulfated sialyl Lewis x capped O- and N-glycans, Blood. 114 (3) (2009) 733–741.
[41] H.B. Wood, G. May, L. Healy, T. Enver, G.M. Morriss-Kay, CD34 expression patterns during early mouse development are related to modes of blood vessel formation and reveal additional sites of hematopoiesis, Blood. 90 (6) (1997) 2300–2311.
[42] W.F. Glass 2nd, R.C. Briggs, L.S. Hnilica, Use of lectins for detection of electrophoretically separated glycoproteins transferred onto nitrocellulose sheets, Anal. Biochem. 115 (1) (1981) 219–224.
[43] J.Q. Gerlach, M. Kilcoyne, S. Eaton, V. Bhavanandan, L. Joshi, Non-carbohydrate-mediated interaction of lectins with plant proteins, Adv. Exp. Med. Biol. 705 (2011) 257–269.
[44] R. Saldova, M. Kilcoyne, H. Stöckmann, S. Millán Martín, A.M. Lewis, C.M. Tuite, J.Q. Gerlach, M. Le Berre, M.C. Borys, Z.J. Li, N.R. Abu-Absi, K. Leister, L. Joshi, P.M. Rudd, Advances in analytical methodologies to guide bioprocess engineering for bio-therapeutics, Methods 116 (2017) 63–83.
[45] M. Kilcoyne, M.E. Twomey, J.Q. Gerlach, M. Kane, A.P. Moran, L. Joshi, Campylobacter jejuni strain discrimination and temperature-dependent glycome expression profiling by lectin microarray, Carbohydr. Res. 389 (2014) 123–133.
[46] B.L. Schulz, N.H. Packer, N.G. Karlsson, Small-scale analysis of O-linked oligosaccharides from glycoproteins and mucins separated by gel electrophoresis, Anal. Chem. 74 (23) (2002) 6088–6097.
[47] S. Mereiter, A. Magalhães, B. Adamczyk, C. Jin, A. Almeida, L. Drici, M. Ibáñez-Vea, C. Gomes, J.A. Ferreira, L.P. Afonso, L.L. Santos, M.R. Larsen, D. Kolarich, N.G. Karlsson, C.A. Reis, Glycomic analysis of gastric carcinoma cells discloses glycans as modulators of RON receptor tyrosine kinase activation in cancer, Biochim. Biophys. Acta 1860 (8) (2016) 1795–1808.
[48] A.V. Everest-Dass, J.L. Abrahams, D. Kolarich, N.H. Packer, M.P. Campbell, Structural feature ions for distinguishing N- and O-linked glycan isomers by LC-ESI-IT MS/MS, J. Am. Soc. Mass Spectrom. 24 (6) (2013) 895–906.
[49] Y. Liu, R. McBride, M. Stoll, A.S. Palma, L. Silva, S. Agravat, K.F. Aoki-Kinoshita, M.P. Campbell, C.E. Costello, A. Dell, S. M. Haslam, N.G. Karlsson, K.H. Khoo, D. Kolarich, M.V. Novotny, N.H. Packer, R. Ranzinger, E. Rapp, P.M. Rudd, W. B. Struwe, M. Tiemeyer, L. Wells, W.S. York, J. Zaia, C. Kettner, J.C. Paulson, T. Feizi, D.F. Smith, The minimum information required for a glycomics experiment (MIRAGE) project: improving the standards for reporting glycan microarray-based data, Glycobiology (2016) [Epub ahead of print].